Laminar Burning Velocities and Transition to Unstable Flames in $H_2/O_2/N_2$ and $C_3H_8/O_2/N_2$ Mixtures

S. KWON, L.-K. TSENG, and G. M. FAETH*
Department of Aerospace Engineering, The University of Michigan, Ann Arbor, MI 48109-2140 USA

Effects of positive flame stretch on laminar burning velocities, and conditions for transition to unstable flames, were studied experimentally for freely propagating spherical flames at both stable and unstable preferential-diffusion conditions. The data base involved new measurements for $H_2/O_2/N_2$ mixtures at values of flame stretch up to 7600 s^{-1}, and existing measurements for $C_3H_8/O_2/N_2$ mixtures at values of flame stretch up to 900 s^{-1}. Laminar burning velocities varied linearly with increasing Karlovitz numbers—either decreasing or increasing at stable or unstable preferential-diffusion conditions—yielding Markstein numbers that primarily varied with the fuel-equivalence ratio. Neutral preferential-diffusion conditions, however, were shifted toward the unstable side of the maximum laminar burning velocity condition that the simplest preferential–diffusion theories associate with neutral stability. All flames exhibited transition to unstable flames: unstable preferential-diffusion conditions yielded early transition to irregular flame surfaces, and stable preferential-diffusion conditions yielded delayed transition to cellular flames by hydrodynamic instability. Conditions for hydrodynamic instability transitions for $H_2/O_2/N_2$ mixtures were consistent with an earlier correlation due to Groff for propane/air flames, based on the predictions of Istratov and Librovich.

NOMENCLATURE

D	mass diffusivity
K	flame stretch
Ka	Karlovitz number, KD_u/S_L^2
L	Markstein length, Eq. 1
Ma	Markstein number, L/δ_D
$O_2/(N_2 + O_2)$	volumetric fraction of O_2 in nonfuel gases
r_f	flame radius
Re	flame Reynolds number, $r_f S_L/\nu_u$
S_L	laminar burning velocity based on unburned gas properties
$S'_{L\infty}$	value of S_L at largest radius observed
t	time
u	gas velocity relative to flame surface

Greek Symbols

α	thermal diffusivity
δA	increment of flame surface area
δ_D	characteristic flame thickness, D_u/S_L
ν	kinematic viscosity
ρ	density
ϕ	fuel-equivalence ratio

Subscripts

b	burned gas properties
cr	condition of transition to unstable flame
max	maximum observed value
u	unburned gas properties
∞	asymptotic condition at large r_f

INTRODUCTION

The results of measurements of spherical laminar premixed flames, freely propagating from spark ignition sources in an initially quiescent gas mixture, are described. Two related issues were of interest: (1) effects of flame stretch on laminar burning velocities, and (2) transitions to unstable flames due to preferential-diffusion and hydrodynamic instability mechanisms. These phenomena are of interest because re-

* Corresponding author.

0010-2180/92/$5.00

cent work has shown that stretch and effects of instability affect the rate of distortion of flame surfaces by turbulence, and thus turbulent burning velocities, for conditions representative of practical turbulent premixed flames [1, 2]. Thus, the findings have application to better understanding effects of preferential diffusion on premixed laminar flame properties and transition to unstable flames, as well as providing quantitative information needed to incorporate effects of stretch in numerical simulations of turbulent premixed flames like those of [3, 4]. Measurements were undertaken using $H_2/O_2/N_2$ mixtures, similar to those used during earlier premixed turbulent flame studies in this laboratory [1–4]. Existing measurements for $C_3H_8/O_2/N_2$ mixtures [5–9] were considered as well, in order to study results for flames having reactant mass diffusion properties more typical of most practical applications than those involving hydrogen.

Following an early proposal of Markstein [10], both simplified asymptotic theories and measurements have suggested a linear relationship between the laminar burning velocity and flame stretch, as follows [7–12]:

$$S_L = S_{L\infty} - LK, \tag{1}$$

where S_L is the relative velocity of the flame with respect to the unburned gas and $S_{L\infty}$ is the value of this velocity when the flame stretch, $K = 0$. The coefficient L is called the Markstein length [11]: it is a measure of the response of the flame to stretch and can be either positive or negative depending on the properties of the reactant mixture. A convenient dimensionless parameter to characterize effects of flame stretch is the Karlovitz number at local flame conditions, Ka, which is the ratio of the characteristic flame residence time, δ_D/S_L, and the characteristic flame stretch time, K^{-1}, or [12, 13]:

$$\mathrm{Ka} = K\delta_D/S_L. \tag{2}$$

During the present study, δ_D was based on unburned gas properties and a characteristic mass diffusivity (for reasons to be discussed later), as follows:

$$\delta_D = D_u/S_L. \tag{3}$$

Substituting Eqs. 2 and 3 into Eq. 1, and rearranging, then yields

$$S_{L\infty}/S_L = 1 + \mathrm{MaKa} \tag{4}$$

where Ma is the Markstein number, defined as follows:

$$\mathrm{Ma} = L/\delta_D. \tag{5}$$

The main issues are whether $S_{L\infty}/S_L$ varies linearly with Ka according to Eq. 4 (implying that Ma is independent of Ka, that is, that the Markstein length is proportional to the characteristic flame thickness), what is the range of Ka where linearity is observed if it is observed at all (e.g., large Ka implies approach to extinction conditions where the variation of S_L with Ka is expected to change), and how do the properties of the reactant mixture affect Ma (particularly the condition where Ma changes sign which represents the boundary between stable and unstable laminar flames)?

Past work has sought to address these issues experimentally, due to the uncertainties of applying simplified theories involving global treatments of chemistry to practical flames. Deshaies and Cambray [7], Law et al. [8], and Searby and Quinard [9] consider steady flames stabilized in a stagnating flow; however, this approach involves large uncertainties due to problem of definitively specifying S_L and Ka from measurements of flow structure [7, 9]. Searby and Quinard [9] examined two other methods as well: a global method based on the amplitude response of the flame to a periodic shear flow, and an indirect method that relates Ma to the onset of cellular instabilities in downward-propagating plane flames. However, both these methods required significant analysis, invoking results of simplified theories [11], so that alternative measurements are needed to evaluate the findings.

The measurements of effects of stretch on laminar burning velocities considered during the present study involved unconstrained outwardly propagating spherical flames due to the relative ease of directly measuring both K and S_L for this flame configuration. For example, the stretch of a premixed flame is defined in the context of a thin flame surface element of

incremental area, δA, as follows:

$$K = d \ln(\delta A)/dt, \tag{6}$$

where changes of δA are observed in a Lagrangian reference frame that moves with the flame surface, that is, the boundary of δA moves tangentially to the flame surface at the local tangential velocity of the gas [12–14]. Expressions for K are complex for general flame geometries and velocity fields; however, for an unconstrained spherical laminar premixed flame propagating at constant pressure away from an ignition source, with negligible motion of the burned gas, Eq. 6 becomes [14]

$$K = (2/r_f)\, dr_f/dt, \tag{7}$$

where r_f is the instantaneous flame radius (taking K to be positive when the center of curvature is within the products). For similar conditions, the laminar burning velocity based on unburned gas properties is given by

$$S_L = (\rho_b/\rho_u)\, dr_f/dt. \tag{8}$$

Because dr_f/dt is more or less fixed for typical gas mixtures, Eq. 7 indicates that effects of flame stretch can best be observed when r_f is small, as long as effects of ignition disturbances can be controlled. In fact, Palm-Leis and Strehlow [5] and Fristrom [6] have observed variations of S_L at small r_f for propane–air flames, indicative of effects of flame stretch, followed by asymptotic approach toward a constant value, $S_{L\infty}$, at large r_f where K becomes small. Additionally, the results of Refs. 5 and 6 show that significant effects of flame stretch on laminar burning velocities can be observed for values of r_f that are significantly greater than characteristic flame thicknesses, which helps to control uncertainties due to resolution of the flame position. Thus, the method is direct and provides reasonable control of experimental uncertainties; its main limitation is that only conditions of positive stretch can be studied.

Flame stretch influences laminar burning velocities through preferential diffusion of heat and mass [11, 13]. Within the thin-flamelet regime, this can cause instability of the flame surface depending upon the sign of the Markstein number. If the Markstein number is negative, the laminar burning velocity increases as the flame stretch increases through Eq. 4; then bulges in a nearly plane flame surface that are concave (convex) toward the combustion products have positive (negative) stretch, analogous to Eq. 7 for spherical flames, so that the bulges grow and the flame is unstable. Conversely, if the Markstein number is positive, the laminar burning velocity decreases with increasing stretch, and similar bulges in the flame surface become smaller so that the flame is stable. These effects can involve preferential diffusion of mass with respect to heat, yielding diffusive-thermal instability [11, 15, 16], preferential diffusion of one reactant with respect to another, yielding diffusive-diffusive instability (more commonly called preferential-diffusion instability [10, 17]), or both. Present observations of these effects will be termed preferential-diffusion instability, to include any combination of diffusive-thermal and diffusive–diffusive phenomena, because it was not possible to firmly identify the specific mechanism. In particular, transitions between stable and unstable conditions were not associated with maximum values of either the flame temperature or the laminar burning velocity with variations of fuel-equivalence ratio—conditions that are normally associated with these transitions for the simplest diffusive-thermal and diffusive-diffusive instability theories [10, 11, 15–17].

Even at neutral and stable preferential diffusion conditions when effects of buoyancy are small (eliminating Rayleigh–Taylor instabilities), laminar flames still are subject to hydrodynamic instability [10, 11]. The mechanism of hydrodynamic instability involves acceleration of the denser reactants toward the less dense combustion products. Markstein [18, 19] presents an early analysis of this instability mechanism, treating the flame surface as a density discontinuity, which has been extended to propagating spherical flames by Istratov and Librovich [20]. However, hydrodynamic instability generally is dominated by effects of preferential diffusion for laboratory-scale experiments, and only a few observations of hydrodynamic instability by Groff [21] and references cited therein have been reported. Hydrodynamic instabilities were observed for

$H_2/O_2/N_2$ mixtures during the present investigation, however, providing an opportunity to extend the findings of Refs. 20 and 21 and to examine the interaction between preferential-diffusion and hydrodynamic instability mechanisms.

To summarize, few quantitative measurements of the effects of stretch on laminar burning velocities, and experimental studies of the interaction between preferential-diffusion and hydrodynamic instabilities, are available. Thus, the objectives of the present investigation were to consider: (1) effects of positive stretch on laminar burning velocities for both stable and unstable preferential-diffusion conditions, and (2) conditions for transition to unstable flames by preferential-diffusion and hydrodynamic mechanisms, while comparing the latter with the findings of Refs. 20 and 21. The data base was limited to unconstrained outwardly propagating spherical flames, considering present measurements for $H_2/O_2/N_2$ mixtures, as well as those of Palm-Leis and Strehlow [5], Fristrom [6] and Groff [21] for $C_3H_8/O_2/N_2$ mixtures. In particular, the results for $H_2/O_2/N_2$ mixtures were of interest both because of interest in these mixtures for developing numerical simulations of premixed turbulent flames [3, 4] and relatively simple H_2/O_2 chemistry for theoretical studies of effects of preferential diffusion, while results for $C_3H_8/O_2/N_2$ mixtures help assess whether behavior observed for $H_2/O_2/N_2$ mixtures was unusual due to the large mass diffusivities of hydrogen.

The paper begins with a description of present experimental methods. This is followed by a description of test conditions for both the hydrogen and propane flames. Results are then considered, treating effects of stretch on laminar burning velocities and transition to unstable flames, in turn.

EXPERIMENTAL METHODS

Apparatus

The present experiments for $H_2/O_2/N_2$ mixtures were carried out using a chamber developed by Groff [21], which also was used during earlier turbulent premixed flame studies in this laboratory [1, 3]. The chamber is quasispherical, with a volume of 0.011 m^3 and a 260-mm cross-sectional diameter at the center. Optical access is provided by two 92-mm-diameter quartz windows mounted opposite one another in the end caps of the chamber. The chamber has a maximum operating pressure of 3400 kPa (34 atm).

The combustible mixture was prepared within the chamber by adding gases to appropriate partial pressures to reach an initial pressure of 3 atm for all tests. The gases were then mixed using fans within the chamber whose normal function is to provide a turbulent combustion environment [3]. However, present tests were in a quiescent environment, so that fan operation was ended and the mixture was allowed to become motionless prior to ignition. After combustion was complete, the chamber was vented to the laboratory exhaust system. The chamber was then purged with dry air to remove condensed water prior to refilling for the next test.

The ignition system was improved from earlier work [1, 3, 21] because it was necessary to observe small radius flames in order to obtain results at high values of stretch (up to 7500 s^{-1}). The present system involved spark ignition at the center of the vessel using electrodes extending from the top and bottom. One electrode was fixed while the other could be moved with a micrometer having a positioning accuracy of 10 μm. The tips of the electrodes were fine wires (tungsten, having a diameter of 250 μm and a free length of 25 mm), with a spark gap of 500 μm. Spark energy was supplied by a high-voltage capacitor discharge circuit with a variable capacitance (100–5000 pF) and voltage (3–5 kV), and a discharge time of roughly 5 μs. Spark energies were adjusted by trial so that they were close to the minimum ignition energy (5–20 mJ), in order to minimize effects of initial flame acceleration by excessive spark energies.

Instrumentation

Measurements involved observing the flames using shadowgraph and schlieren motion picture photography. The shadowgraph and schlieren systems were based on a 100-W mer-

cury short arc lamp (ARC, HSA-150 HP), with the light collimated by a pair of f6 parabolic reflectors having focal lengths of 1220 mm. The flame images were recorded using a 16-mm high-speed motion picture camera (Hycam, Model K20 S4E) operating at 5000 pictures per second with a 1/10 shutter to yield an exposure time of 20 μs. Kodak Tri X reversal film was used for the photographs. The framing rate of the camera was sensed electronically so that the triggering pulse to the ignitor occurred when the proper framing rate was reached. Both the framing rate and the ignition pulse were recorded on a digital oscilloscope (LeCroy 9400A) so that the film records could be synchronized.

The film records were measured by projecting them using an Athena model 224 (MK VIII) projector. The overall magnification of the projected images was 4:1. The flames were generally spherical (maximum and minimum diameters were within 10% of the mean diameter); however, the diameters were measured horizontally to minimize effects of flame surface disturbances due to the presence of the spark electrodes. The shadowgraphs yielded the sharpest images of the flame surface; therefore, they were used for the measurements. This provided an overall resolution of the flame diameter within 100 μm.

Measurements of laminar burning velocities only were carried out for relatively small flames (diameters less than 44 mm). Within this region, the volume of burned gas was less than 1% of the total chamber volume and the chamber pressure was constant within 3%, which was confirmed by measurements with a pressure transducer. Additionally, laser velocimeter measurements in the unburned gas during flame propagation indicated that velocities corresponded to behavior anticipated for unconfined freely propagating spherical flames [3]. Thus, laminar burning velocities based on unburned gas properties were found from Eq. 8, assuming constant pressure combustion with the reactant gas temperature equal to the initial temperature and negligible motion of the burned gas. The density ratio in Eq. 8 was found assuming thermodynamic equilibrium in the combustion products using the Gordon and McBride [22] algorithm. The experimental uncertainties (95% confidence) of dr_f/dt and S_L were less than 5% and 7%, respectively. The higher uncertainty of S_L reflects estimated uncertainties of the density ratio in Eq. 8, as well as potential effects of the slight chamber pressure increase and radiative cooling of the burned gas [23]. The corresponding uncertainties of flame stretch from Eq. 7 were less than 15%. Finally, values of the Karlovitz number were found by eliminating δ_D between Eqs. 2 and 3 to yield

$$\mathrm{Ka} = KD_u/S_L^2. \tag{9}$$

Evaluating Ka from Eq. 9 involved experimental uncertainties (95% confidence) less than 20%.

TEST CONDITIONS

H_2 / O_2 / N_2 Mixtures

Present tests for $H_2/O_2/N_2$ mixtures were limited to an initial pressure within the combustion chamber of 3 atm, similar to Refs. 1 and 3; as noted earlier, combustion chamber pressures remained nearly constant during the period when flame properties were measured. Combined considerations of experimental uncertainties, and a desire to reach Ka ~ 0.1 to see reasonable effects of flame stretch, implied that S_L should generally be less than 1.5 m/s. Thus, it was necessary to dilute the mixtures with nitrogen in order to reduce S_L in regions where it reached a maximum with respect to variations of ϕ.

Table 1 is a summary of specific conditions considered during the present investigation. Volumetric fractions of O_2 in the nonfuel gas, $O_2/(N_2 + O_2)$, of 0.125, 0.140, 0.150, and 0.210 (the last corresponding to air) were studied, to match conditions of earlier work [1, 3]. Two test series were considered: one at $O_2/(N_2 + O_2) = 0.125$, and a second having nearly constant laminar burning velocities at the maximum radius of observations, $S'_{L\infty} = 1.23 \pm 0.12$ m/s. Both series involved fuel-equivalence ratios in the unstable ($\phi = 1.00$ and 1.41) and stable ($\phi = 1.80$–4.83) preferential-diffusion instability regimes.

As noted earlier, values of ρ_u/ρ_b in Table 1 were found from Ref. 22. The transport prop-

TABLE 1

Summary of $H_2/O_2/N_2$ Test Conditions[a]

ϕ (−)	$O_2/(N_2 + O_2)$ (−)	ρ_u/ρ_b (−)	α_u (mm^2/s)	ν_u (mm^2/s)	$S'_{L\infty}$ (m/s)	$S_{L\infty}$ (m/s)	$\delta_{D\infty}$ (μm)	K_{max} (s^{-1})	Ma (−)
1.00	0.140	5.88	12.6	5.6	1.11	1.02	25	7600	−1.8
1.00	0.125	5.55	11.5	5.0	0.69	0.54	47	5100	−2.7
1.41	0.125	5.29	13.2	5.5	1.35	1.35	19	7100	0.0
1.80	0.125	5.07	14.5	6.5	1.44	1.45	18	6100	2.0
2.25	0.125	4.83	15.7	6.8	1.35	1.37	19	5000	2.7
2.78	0.125	4.59	17.8	7.3	1.14	1.21	21	2900	4.7
3.27	0.125	4.38	19.3	7.8	0.98	1.16	22	1500	8.1
3.61	0.150	4.53	21.9	8.6	1.26	1.42	18	3000	6.7
4.83	0.210	4.38	28.0	9.6	1.28	1.64	15	1900	13.3

[a] Initial mixture pressure and temperature of 3 atm and 298 ± 3 K. D_u = 25.4 mm^2/s for all conditions.

erties, α_u and ν_u, were computed for the unburned gas mixture using the methods of Brokaw, and Mason and Saxena, cited in Ref. 24, based on pure gas properties from Ref. 25. The mass diffusivity, D_u, was taken to be the binary diffusivity of hydrogen and nitrogen found from Ref. 24. This diffusivity was used to define Ka and δ_D for scaling purposes, because present results did not identify a specific preferential-diffusion mechanism. Values of $S'_{L\infty}$ were found directly at the largest radius where observations were made, while $S_{L\infty}$ values were found by extrapolation to Ka → 0, as discussed later. Characteristic flame thicknesses, $\delta_{D\infty}$, are found using $S_{L\infty}$ in Eq. 3. The resulting characteristic flame thicknesses are in the range 15–47 μm, which are roughly two orders of magnitude smaller than the smallest values of r_f that were considered (2–3 mm). These sharp gradients help minimize uncertainties of associating shadowgraph images with the flame position [6]. Maximum values of flame stretch were in the range 1500–7600 s^{-1} over all the test conditions; these values of K are generally smaller than values approaching extinction conditions, which is a natural consequence of avoiding measurements near small spark kernals involving minimum ignition energies [23]. Values of Ma, found as described later, also are summarized in Table 1.

C_3H_8 / O_2 / N_2 Mixtures

Existing measurements considered for $C_3H_8/O_2/N_2$ mixtures involved results of Palm-Leis and Strehlow [5], Fristrom [6], and Groff [21] for freely propagating spherical flames, and Deshais and Cambray [7] for steady flames stabilized in a stagnation flow. The measurements of Groff [21] employed the same apparatus as present measurements and were limited to conditions for the onset of hydrodynamic instability in propane–air flames. Results from the remaining investigations were used to study effects of stretch on laminar burning velocities; original sources, and references cited therein, should be consulted for the details of these experiments.

Table 2 is a summary of test conditions from Refs. 5–7 that were used to study effects of stretch on S_L for $C_3H_8/O_2/N_2$ mixtures. The freely propagating flames all involve propane–air mixtures, with reported measurements of dr_f/dt as a function of r_f used to find S_L and Ka in the same manner as the present experiments (finding ρ_u/ρ_b from Ref. 22 as before). The value of D_u was taken to be the binary diffusivity of propane in nitrogen from Ref. 24. The resulting characteristic flame thicknesses are in the range 28–147 μm, which still are small in comparison to the smallest values of r_f considered (5–15 mm). Maximum values of flame stretch were in the range 200–900 s^{-1} over the data base, which are an order of magnitude smaller than the hydrogen flames; nevertheless, values of Ka were comparable due to smaller values of S_L. As before, avoiding conditions where the spark discharge was a factor implies that maximum values of K are not very close to extinction conditions.

The relevant properties of the steady flame results of Deshaies and Cambray [7] also are

TABLE 2

Summary of $C_3H_8/O_2/N_2$ Test Conditions[a]

ϕ (−)	$O_2/(N_2 + O_2)$ (−)	ρ_u/ρ_b (−)	$S_{L\infty}'$ (m/s)	$S_{L\infty}$ (m/s)	$\delta_{D\infty}$ (μm)	K_{max} (s^{-1})	Ma (−)
Palm-Leis and Strehlow [5]:							
0.775	0.210	6.97	0.21	0.22	51	200	5.5
0.850	0.210	7.35	0.26	0.26	43	300	4.3
0.985	0.210	7.93	0.35	0.35	32	500	4.3
1.160	0.210	8.06	0.41	0.41	28	500	4.3
1.362	0.210	7.83	0.38	0.38	30	500	3.1
1.548	0.210	7.62	0.26	0.26	43	300	0.6
1.708	0.210	7.40	0.14	0.13	87	300	−1.8
1.878	0.210	7.14	0.088	0.077	147	200	−2.2
Fristrom [6]:							
1.000	0.210	7.94	0.40	0.40	28	900	5.0
Deshaies and Cambray [7]:							
0.800	0.153	—	—	0.095	119	24	8.0

[a] Initial mixture at normal temperature and pressure. D_u = 11.3 mm^2/s for all conditions.

summarized in Table 2. In this case, values of $S_{L\infty}$, S_L, and K were taken directly from Table 1 and Fig. 4 of Ref. 7, and reduced using the same value of D_u as the rest of propane flame measurements. For these results, the maximum value of K was roughly an order of magnitude smaller than the freely propagating flames, 24 s^{-1}, although nitrogen dilution yielded small values of S_L as well, so that values of Ka were comparable.

No estimates of experimental uncertainties are reported in Refs. 5–7; however, the results for the freely propagating flames seem comparable to present measurements. Then, considering the uncertainties of transferring data from small plots, it is estimated that the uncertainties of S_L and Ka are less than 10% and 30%, respectively.

LAMINAR BURNING VELOCITIES

H_2 / O_2 / N_2 Mixtures

Flame radius as a function of time for $H_2/O_2/N_2$ mixtures is plotted in Fig. 1 for various fuel-equivalence ratios at $O_2/(N_2 + O_2) = 0.125$. These, and all other results, are averages of at least four tests in order to smooth the data. Disturbed flame surfaces were observed at $\phi = 1.00$ and 1.41, as indicated on the plots: these transitions to disturbed surface are due to preferential-diffusion instability, transitions due to hydrodynamic instability occur for values of r_f larger than those illustrated in Fig. 1. Transitions to unstable flames will be discussed later; fortunately, they occurred at sufficiently large values of r_f that effects of flame stretch on laminar burning velocities could still be observed. Effects of

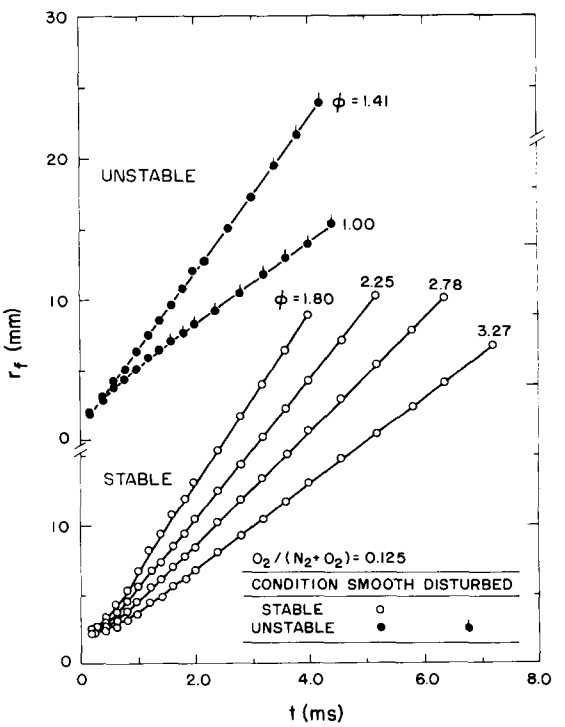

Fig. 1. Flame radius as a function of time for $H_2/O_2/N_2$ mixtures: $O_2/(N_2 + O_2) = 0.125$.

preferential diffusion can be seen from the variation of the slopes of the plots (which are proportional to S_L through Eq. 8). Thus, the slopes increase (decrease) with increasing r_f (decreasing K) for stable (unstable) conditions, tending toward constant values at large r_f where K approaches zero (barring effects of transition to an irregular flame surface).

Reactant properties at the transition between stable and unstable preferential-diffusion conditions in Fig. 1 are not in agreement with the simplest diffusive–diffusive or diffusive–thermal instability concepts. For example, transition from stable to unstable conditions for diffusive–diffusive instability is normally associated with the maximum laminar burning velocity condition [10, 17]. For $H_2/O_2/N_2$ flames, the laminar burning velocity reaches a maximum near $\phi = 1.8$ [23], which was taken to be a near-neutral preferential-diffusion condition during earlier work [1, 3]. However, present results at $\phi = 1.80$ clearly are representative of stable behavior, while results at $\phi = 1.41$, well away from the maximum value of S_L, yield S_L relatively independent of r_f, which implies near-neutral (though slightly unstable) behavior. Additionally, diffusive-thermal instability theories normally involve model flame systems where the maximum adiabatic flame temperature and laminar burning velocity conditions coincide, and yield transition to unstable conditions near the maximum laminar flame temperature, or more recently, somewhat shifted toward the unstable side of the maximum laminar flame temperature [11, 15]. None of these requirements or results are satisfied for present $H_2/O_2/N_2$ mixtures: the adiabatic flame temperature is a maximum near $\phi = 1$, which is well below $\phi = 1.8$, where the laminar burning velocity reaches a maximum, while the near-neutral condition near $\phi = 1.41$ is shifted toward the stable side of the maximum temperature condition (although it is toward the unstable side of the maximum laminar burning velocity condition). In view of these observations, and similar difficulties for $C_3H_8/O_2/N_2$ flames, it seems prudent to refer to present behavior more generically as effects of preferential-diffusion instability without specific reference to the scalar properties that are preferentially diffused.

The measurements of flame radius as a function of time were used to compute S_L as a function of r_f from Eq. 8. The results are illustrated in Fig. 2 for $O_2/(N_2 + O_2) = 0.125$ and in Fig. 3 for $S'_{L\infty} = 1.23 \pm 0.12$ m/s. As before, unstable conditions, where the flame surface was irregular, are marked on the figures. As discussed earlier, S_L increases (decreases) with increasing r_f for stable (unstable) conditions, tending toward a constant value at large r_f, where K becomes small.

The results of Figs. 2 and 3 all involve finite values of K so that the maximum observed values of the laminar burning velocities $S'_{L\infty}$ differ from the true asymptotic value when $K = 0$, $S_{L\infty}$. The value of $S_{L\infty}$ was found through Eq. 4 by plotting $S'_{L\infty}/S_L$ as a function of Ka, considering results only for stable flame surfaces in cases where transition was observed. Plots of this type are linear, as discussed later, so that extrapolation to Ka = 0 yielded $S'_{L\infty}/S_{L\infty}$ and thus $S_{L\infty}$ as summarized in Table 1. For near-neutral conditions ($\phi = 1.41$–2.25), $S'_{L\infty}$ and $S_{L\infty}$ agree within a few percent because effects of flame stretch are small; however, there are differences between

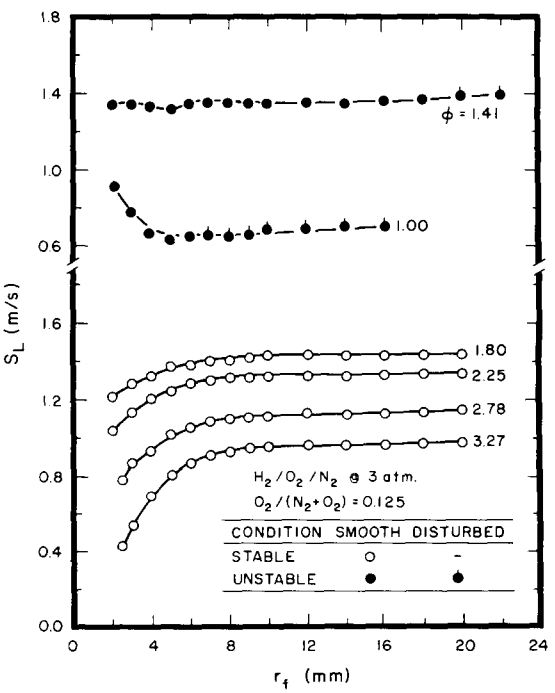

Fig. 2. Laminar burning velocities as a function of flame radius for $H_2/O_2/N_2$ mixtures: $O_2/(N_2 + O_2) = 0.125$.

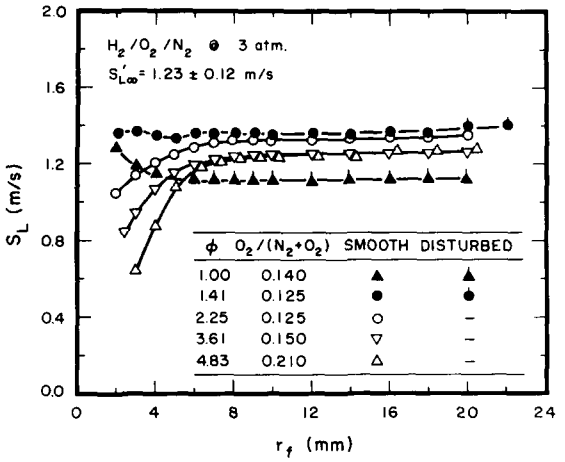

Fig. 3. Laminar burning velocities as a function of flame radius for $H_2/O_2/N_2$ mixtures: $S'_{L\infty} = 1.23 \pm 0.12$ m/s.

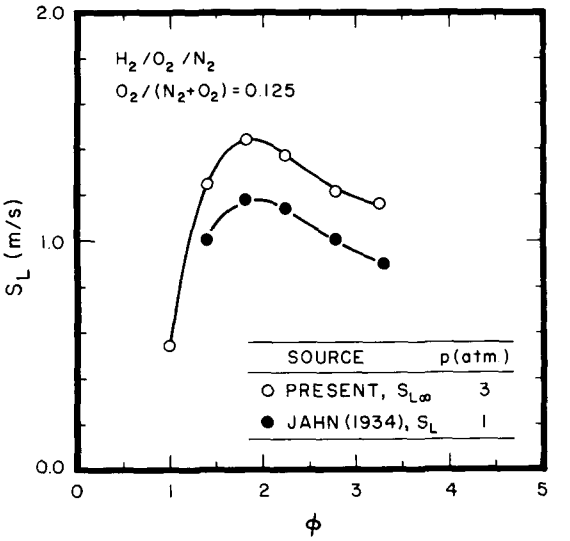

Fig. 4. Laminar burning velocities as a function of fuel-equivalence ratio for $H_2/O_2/N_2$ mixtures: $O_2/(N_2 + O_2) = 0.125$. Measurements of Jahn (1934), cited in Lewis and von Elbe [23], and present study.

the two of up to 28% at other conditions. The unstable conditions at $\phi = 1$ are particularly interesting because $S_{L\infty}$ is significantly lower than $S'_{L\infty}$, even though the observed values of S_L are relatively uniform (or even increase slightly) for the larger values of r_f (see Figs. 2 and 3). This occurs due to the onset of instability which yields irregular flame surfaces over the same range of r_f, enhancing the burning velocity to compensate for reductions in S_L with increasing r_f had the flame surface remained smooth (the two effects fortuitously yield a relatively constant apparent value of S_L over the unstable range of r_f).

It is of interest to compare present measurements of $S_{L\infty}$ with results available in the literature. This can be done for $O_2/(N_2 + O_2) = 0.125$, based on the extensive measurements using Bunsen burner flames at atmospheric pressure of Jahn, cited in Lewis and von Elbe [23]. The results are illustrated in Fig. 4, where the measurements of Jahn are denoted as S_L because the appropriate values of K are unknown (although effects of finite K should be small near the neutral-stability condition, ϕ ca. 1.4). The trends of the two sets of measurements are similar, with the maximum laminar burning velocity reached near $\phi = 1.8$. Present values of $S_{L\infty}$ are roughly 20% higher than the measurements of Jahn; however, this is expected due to the difference in pressure from 1 to 3 atm, based on the known variation of S_L with pressure for hydrogen fueled flames [23].

The values found for $S_{L\infty}$ were used to plot $S_{L\infty}/S_L$ as a function of Ka, as suggested by Eq. 4. The results are illustrated in Figs. 5 and 6 for $O_2/(N_2 + O_2) = 0.125$ and $S'_{L\infty} = 1.23 \pm 0.12$ m/s, respectively. Conditions where disturbed flame surfaces were observed have

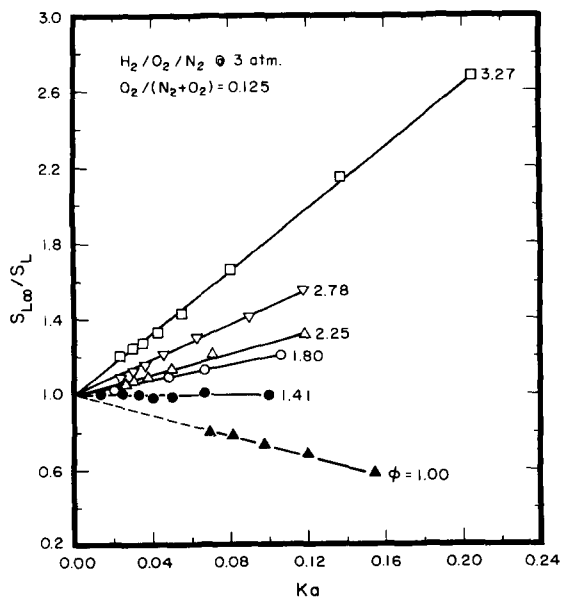

Fig. 5. Laminar burning velocities as a function Karlovitz number for $H_2/O_2/N_2$ mixtures: $O_2/(N_2 + O_2) = 0.125$.

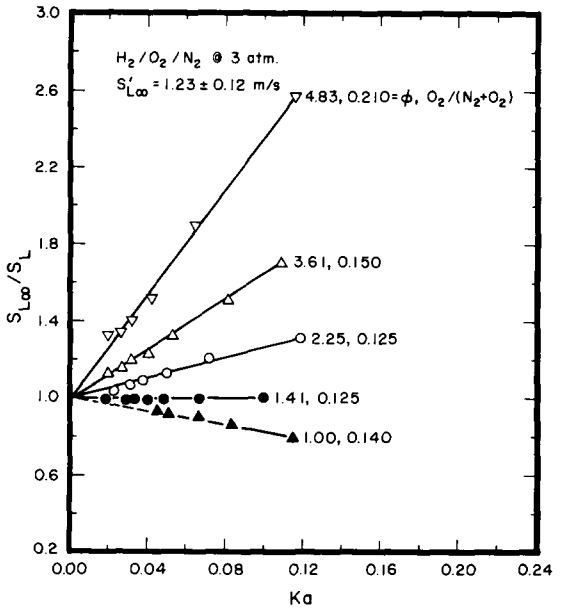

Fig. 6. Laminar burning velocities as a function of Karlovitz number for $H_2/O_2/N_2$ mixtures: $S'_{L\infty}$ = 1.23 ± 0.12 m/s.

been omitted, with the extrapolation of the fit of the data to the origin shown as a dashed line in this region. Some points near the origin have been omitted as well, to avoid overlapping symbols. The behavior of both test series is the same, with the measurements yielding a linear relationship between $S_{L\infty}/S_L$ and Ka, as suggested by Eq. 4. The slope of these plots is the Markstein number, which clearly is independent of Ka over the range of present measurements (Ka < 0.21), although it should be recalled that present conditions are not very close to extinction conditions. This behavior suggests that the Markstein length scales with the characteristic flame thickness (see Eq. 5), which is plausible because both are representative of distances over which scalar transport occurs [10, 11]. The behavior for various values of ϕ is seen to be quite regular, with the slopes of the curves (Ma) progressively increasing from negative values at ϕ = 1, through the horizontal near-neutral condition at ϕ = 1.41, to relatively large positive values at the highest values of ϕ considered. The corresponding variations of $S_{L\infty}/S_L$ are substantial, ranging from 0.5 to 2.7 even for Ka < 0.21: flame stretch clearly has a very significant effect on the laminar buring velocities of $H_2/O_2/N_2$ mixtures, except near the neutral preferential-diffusion stability condition.

The present values of Ma found from the results of Figs. 5 and 6 are summarized in Table 1 and also are plotted as a function of ϕ in Fig. 7. The present values of Ma vary nearly linearly with ϕ, with effects of nitrogen dilution not being very significant in comparison to experimental uncertainties (estimated (95% confidence) to be less than 40%). It should be recalled, however, that the present range of ϕ does not extend to conditions near flammability limits where the behavior of Ma is likely to change. For example, at $O_2/(N_2 + O_2)$ = 0.21 and 0.125, ϕ is ca. 0.1 and 0.2 at the lean limit, and ca. 7.1 and 4.3 at the rich limit at atmospheric pressure [23], with these limits likely to be broader at 3 atm.

Recent measurements of Ma for $H_2/O_2/N_2$ mixtures by Searby and Quinard [9] also are plotted in Fig. 7. They clearly are not in very good agreement with present observations, both with respect to the trends of Ma with ϕ and the value of ϕ for transition between stable and unstable flames. The measurements in Ref. 9 were obtained by associating the appearance of cellular structures with the Markstein number based on a simplified diffusive-thermal instability analysis. As noted earlier, such simplified analyses are questionable

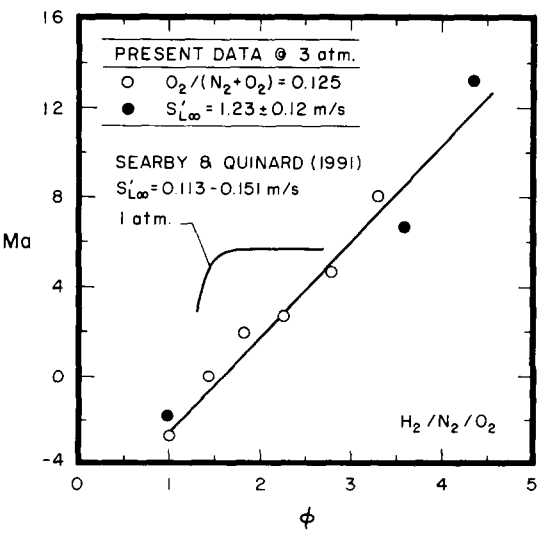

Fig. 7. Markstein numbers as a function of fuel-equivalence ratio for $H_2/O_2/N_2$ mixtures. Measurements of Searby and Quinard [9] and present study.

for $H_2/O_2/N_2$ mixtures because conditions of maximum temperature and laminar burning velocity are widely separated in terms of ϕ. Additionally, Froude number effects were involved in the evaluation of Ma in Ref. 9, which can introduce problems of interactions between Rayleigh–Taylor (buoyancy) and preferential-diffusion instability. Thus, it appears that the indirect method of Ref. 9 to find Ma requires additional development, with the propagating spherical flame method favored for the present due to its directness and simplicity.

$C_3H_8 / O_2 / N_2$ Mixtures

The properties of $H_2/O_2/N_2$ mixtures are not very typical of most practical flame systems, due to the wide separations between maximum flame temperature and laminar burning velocity conditions, and the unusually large mass diffusivity of hydrogen. This prompted consideration of effects of stretch on the laminar burning velocities of $C_3H_8/O_2/N_2$ mixtures, based on reconsideration of the measurements of Palm-Leis and Strehlow [5], and supplemented by the measurements of Fristrom [6] and Deshaies and Cambray [7]. The freely propagating spherical flame data [5, 6] was processed in the same manner as the hydrogen flames, while the relevant results were obtained directly from data reported for the stagnation point flame [7].

The values of $S'_{L\infty}$ and $S_{L\infty}$ for the propane flames are summarized in Table 2. The $S_{L\infty}$ for propane–air flames from Palm-Leis and Strehlow [5] also are plotted as a function of ϕ in Fig. 8, along with other measurements in the literature for steady laminar flame configurations [24–32]. The results of Refs. 24–32 involve unknown levels of stretch but generally agree with respect to the trends of S_L with ϕ and yield maximum values of S_L within 10% of each other. The maximum values of $S_{L\infty}$ from [5] agree with the rest as well; however, these results appear to be shifted toward larger values of ϕ, for example, the maximum laminar burning velocity occurs at roughly $\phi = 1.2$ rather than roughly $\phi = 1.1$ for the steady flame configurations. Effects of flame stretch cannot explain this shift; for example, $C_3H_8/O_2/N_2$ mixtures are stable with respect to preferential diffusion for $\phi < 1$ so that strain

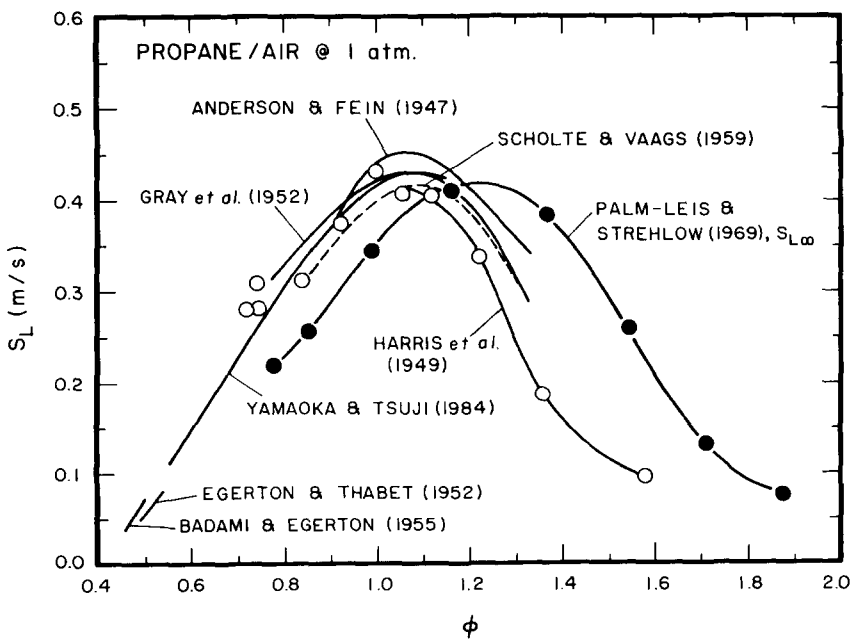

Fig. 8. Laminar burning velocities as a function of fuel-equivalence ratio for propane/air mixtures. Measurements of Palm-Leis and Strehlow [5], Harris et al. [26], Yamaoka and Tsuji [27], Anderson and Fein [28], Scholte and Vaags [29], Gray et al. [30], Egerton and Thabet [31], and Bodami and Egerton [32].

should reduce S_L from $S_{L\infty}$ in this region, not increase it, as seen in Fig. 8. This suggests that an error has been made when computing ϕ in Ref. 5. Fortunately, properties like ρ_u/ρ_b do not vary rapidly with ϕ for propane–air flames (see Table 2), so that effects of K on S_L can still be evaluated for these flames, noting that the values of ϕ may be shifted somewhat.

The variation of $S_{L\infty}/S_L$ with Ka for $C_3H_8/O_2/N_2$ mixtures is plotted in Fig. 9 for various values of ϕ, considering results from Refs. 5–7. The general similarity of the results for propane in Fig. 9, and those for hydrogen in Figs. 5 and 6, is striking. The main overall difference is that unstable conditions occur for fuel-rich mixture ratios for propane and fuel-lean mixture ratios for hydrogen, which is consistent with general preferential-diffusion ideas based on the relative diffusion rates of the fuel and oxidant [17]. Similar to hydrogen, the slopes of the plot (the Markstein numbers) are constant over the test range, Ka < 0.37, although, as noted earlier, these conditions were not very close to extinction conditions where behavior might be different. The measurements of Fristrom [6] are in reasonably good agreement with those of Palm-Leis and Strehlow [5], in spite of the probable errors in specifying ϕ for the latter measurements. This is fortuitous because the measurements of Fristrom [6] are in a region where the results are relatively insensitive to variations of ϕ. In contrast, the stagnation flame measurements of Deshaies and Cambray [7] exhibit greater sensitivity of S_L to Ka than the rest; this can be attributed to the uncertainties of the method pointed out by Searby and Quinard [9], as well as effects of interpretation of the measurements using a simplified flame structure theory. Aside from the measurements of Deshaies and Cambray [7], the propane flames exhibit a regular variation of the sensitivity of S_L to ϕ, with the slope of the plots progressively increasing as ϕ decreases. Additionally, the variations of $S_{L\infty}/S_L$ are quite large, in the range 0.6–3.1, even though Ka < 0.37; thus, large effects of stretch on laminar burning velocities are not confined to reactant mixtures where there are

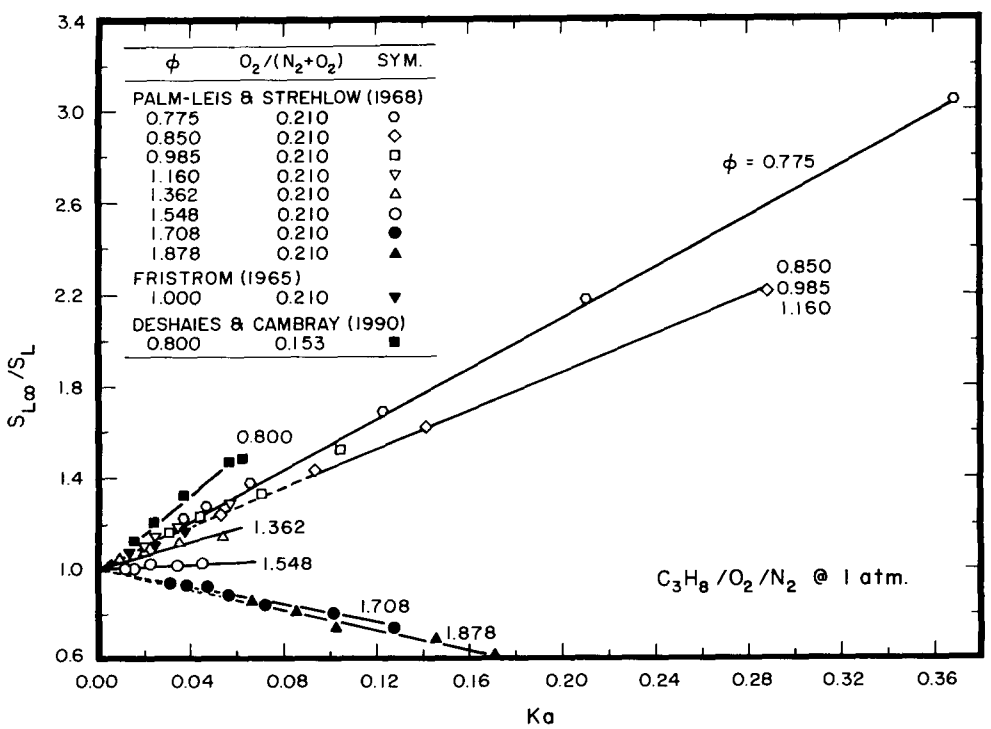

Fig. 9. Laminar burning velocities as a function Karlovitz number for $C_3H_8/O_2/N_2$ mixtures. Measurements of Palm-Leis and Strehlow [5], Fristrom [6], and Deshaies and Cambray [7].

large differences in mass diffusivities between reactant species, like hydrogen-fueled flames.

The values of Ma found from Fig. 8 are summarized in Table 2 and plotted as a function of ϕ in Fig. 10. As noted earlier, the value of Ma from Fristrom [6] is in reasonable agreement with the results of Palm-Leis and Strehlow [5], while the value from Deshaies and Cambray [7] is significantly higher than the rest. Measurements from Searby and Quinard [9] for various levels of nitrogen dilution, based on observations of the onset of cellular instability, also are shown on the plot. These agree with results from Refs. 5 and 6 at low ϕ but suggest a more rapid approach to unstable conditions with increasing ϕ. The problems of the cellular instability approach, discussed in connection with the $H_2/O_2/N_2$ mixtures, are probably the main source of these differences, with potential errors of ϕ in Ref. 5 being a possible contributing factor.

In contrast to the $H_2/O_2/N_2$ flames (Fig. 7), the values of Ma for propane appear to approach limits for stable and unstable conditions at small and large values of ϕ. This behavior may be due to the fact that the test range for the propane–air flames extended closer to the lean and rich flammability limits

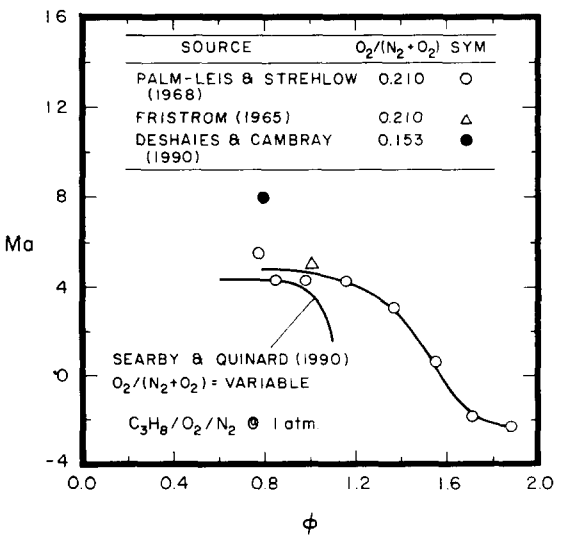

Fig. 10. Markstein numbers as a function of fuel-equivalence ratio for propane–air mixtures. Measurements of Palm-Leis and Strehlow [5], Fristrom [6], Deshaies and Cambray [7], and Searby and Quinard [9].

than the hydrogen flames, for example, for propane–air flames, ϕ is ca. 0.54 and 2.5 at the lean and rich limits at atmospheric pressure [23]. Transition from stable to unstable preferential diffusion conditions (Ma = 0) occurs near $\phi = 1.6$ (and probably slightly lower due to possible errors in reported values of ϕ), which is well above (shifted toward the unstable side) the values of ϕ where the adiabatic flame temperatures and laminar burning velocities reach maximum values, ϕ ca. 1.0 and 1.1. This behavior is in qualitative agreement with predictions from the simplified diffusive-thermal stability theories [11], with more normal behavior for propane than hydrogen flames perhaps following because the values of ϕ where the maximum adiabatic flame temperature and laminar burning velocity are reached are closer together for propane than for hydrogen.

Transition to Disturbed Flames

For unstable preferential-diffusion conditions, present observations of transition to disturbed flames for $H_2/O_2/N_2$ mixtures occurred at relatively small values of r_f and involved irregular wrinkled flames. However, for stable preferential-diffusion conditions, transition occurred at relatively large values of r_f and involved cellular flames, similar to those observed by Groff [21] for propane–air mixtures at stable preferential-diffusion conditions. Following Groff [21], conditions for transition were represented by a critical Reynolds number based on flame speed and radius, and unburned gas properties, $\mathrm{Re}_{cr} = (r_f S_L/\nu_u)_{cr}$.

The appearance of the hydrogen flames at Re less and greater than Re_{cr} can be seen from the shadowgraph photographs of Fig. 11 (on this figure Re_{cr} refers to transition by hydrodynamic instability based on the correlation for stable flames to be discussed in connection with Fig. 12). Results are shown for $\phi = 1.00$, 1.80, and 3.27, which represent unstable, weakly stable, and stable preferential-diffusion conditions, respectively. The photographs for $\mathrm{Re} < \mathrm{Re}_{cr}$ were obtained at nearly the same flame radius (seen as the nearly spherical outer boundary of the dark region near the center of the photograph). At this

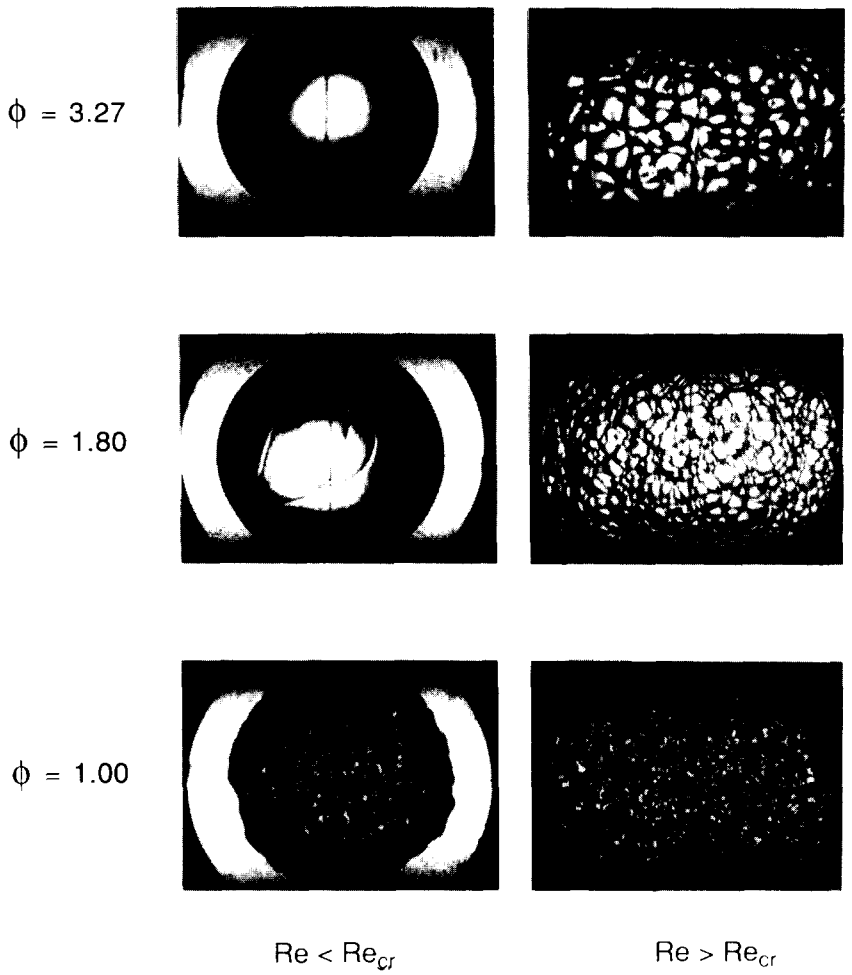

Fig. 11. Shadowgraph photographs of flame surfaces for $H_2/O_2/N_2$ mixtures. Re less and greater than Re_{cr} for stable and unstable preferential diffusion conditions.

condition, the weakly stable flame exhibits some surface disturbances associated with the flame interacting with the ignitor wires; however, the strong action of stability at $\phi = 3.27$ has eliminated such disturbances and the flame surface is smooth. In contrast, the unstable flame ($\phi = 1.00$) has already undergone transition to an irregular flame surface at these conditions by the preferential-diffusion mechanism, even though the flame Reynolds number is lower than values associated with transition by hydrodynamic instability for stable preferential-diffusion conditions.

For $Re > Re_{cr}$ in Fig. 11, only a portion of the flame surface could be observed using the present photographic system. At these conditions, the unstable flame still exhibits irregular distortions of the flame surface. The weakly stable and stable flames, however, now exhibit a somewhat regular cellular pattern. These cellular patterns evolved similar to the film strips illustrated by Groff [21] for propane–air flames, with new cells forming as the flame radius increases and the general size of the cells tending to decrease as the expansion ratio of the flames, ρ_u/ρ_b, increased. Notably, transitions of this type were observed at all test conditions for stable flames ($\phi \geq 1.8$ in Table 1).

It was of interest to determine whether present observations of transitions to cellular flames for hydrogen flames were consistent with transitions observed by Groff [21] for propane flames, and could be correlated in the

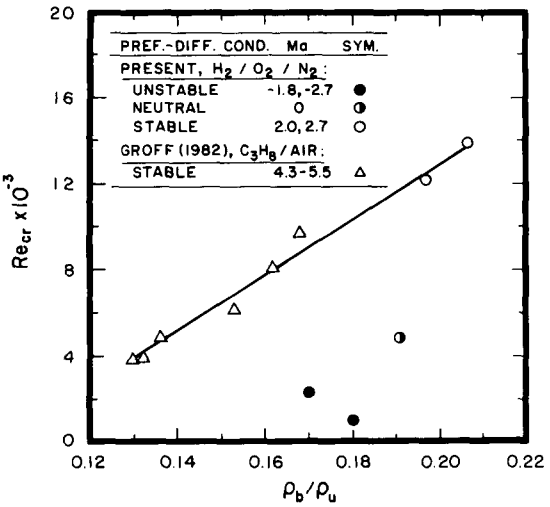

Fig. 12. Critical Reynolds number for transition to unstable flames as a function of expansion ratio. Measurements of Groff [21] and present measurements.

same manner based on the hydrodynamic instability theory of Istratov and Librovich [20]. Unfortunately, these transitions occurred at flame radii that were too large for direct measurements of r_f and S_L at the time of transition, even though the time of transition could be observed from the appearance of cells on the shadowgraph motion picture photographs. Thus, it was necessary to extrapolate results measured when the flames were near the outer edge of the windows, assuming that S_L and dr_f/dt remained constant, to find the flame radius at transition, r_{fcr}. In order to avoid variations of S_L and other properties at large radii, where the unreacted gases have been compressed significantly, these measurements were limited to $r_{fcr} \leq 71$ mm, where the combustion products comprised less than 14% of the chamber volume and the flames are relatively unconstrained. A summary of the data, which includes both stable and unstable preferential-diffusion conditions, appears in Table 3.

Conditions for transition to unstable flames are illustrated in Fig. 12. The results involve Re_{cr} plotted as a function of ρ_u/ρ_b based on the approximate hydrodynamic instability theory of Istratov and Librovich [20]. The measurements include present findings for $H_2/O_2/N_2$ mixtures at both stable and unstable preferential diffusion conditions, as well as the results of Groff [21] for propane–air mixtures at stable preferential diffusion conditions. Values of Ma, as a measure of effects of preferential diffusion to stabilize irregularities of flame surfaces, also are indicated on the plots. Values of Ma for the present measurements are taken from Table 1; those for propane–air flames are taken from Table 2, ignoring effects of pressure (results in Table 2 are for atmospheric pressure while initial pressures of Ref. 21 were in the range 308–1305 kPa) and possible errors in ϕ from Ref. 5.

The results plotted in Fig. 12 for stable preferential-diffusion conditions satisfy a similar correlation for transition to a cellular flame surface, independent of the reactant mixture, which suggests hydrodynamic instability. This apparent universal behavior is somewhat surprising, however, because the mechanism of preferential-diffusion stability is expected to resist the formation of cellular disturbances [12, 15] and the response of S_L to Ka varies significantly over the range of stable conditions, for example, Ma is in the range 2.0–5.5. This can be explained by noting that the mech-

TABLE 3

Conditions for Transition to Unstable Flames for $H_2/N_2/O_2$ Mixtures

ϕ (–)	$O_2/(N_2 + O_2)$ (–)	r_{fcr} (mm)	$S_{L_{cr}}$ (m/s)	Re_{cr} (–)
Preferential diffusion transition to irregular flame surface:				
1.00	0.140	12	1.11	2,400
1.00	0.125	7	0.71	1,000
1.41	0.125	19	1.39	4,800
Hydrodynamic transition to cellular flame surface:				
1.80	0.125	55	1.44	12,200
2.25	0.125	71	1.34	14,000

anism of preferential-diffusion stability is not effective on the scales of the cells observed for hydrodynamic instability. In particular, effects of large Ka and transition to hydrodynamic instability are widely separated in terms of r_f, and reasonably separated in terms of present observations of cell size. For example, hydrodynamic instability tends to distort the flame surface beginning at the largest scale; see the photographs in Ref. 21. Thus, it is possible that hydrodynamic instability is observed when the mechanism of preferential-diffusion stability is no longer strong enough to prevent the formation of cells. However, an effect of Ma on cellular transition cannot be excluded because the data are grouped, with higher values of Ma for the propane flames near the left-hand side of the plot, and lower values of Ma for the hydrogen flames at the right-hand side of the plot. Thus, the apparent correlation for cellular transitions at stable conditions may be affected by parametric variations of Ma. Measurements over a broader range of conditions clearly are needed to resolve interactions between preferential-diffusion effects and transitions to cellular flames.

Results for near-neutral (which is probably slightly unstable) and unstable conditions in Fig. 12 exhibit lower values of Re_{cr} for transition than the stable flames—particularly the most unstable flames at $\phi = 1$. For these conditions, the surface structure does not have the coherent cellular structure that was evident for stable conditions, implying that the mechanism of surface distortion cannot be explained by hydrodynamic instability alone. Additionally, the correlation for hydrodynamic instability yields Re_{cr} much larger than observed for near-neutral and unstable conditions. This behavior is expected based on numerous past observations of preferential-diffusion instability [1, 2, 5, 6, 10–12, 15–17].

CONCLUSIONS

Effects of positive flame stretch on laminar burning velocities, and conditions for transition to unstable flames, were studied based on measurements for freely propagating spherical flames in $H_2/O_2/N_2$ and $C_3H_8/O_2/N_2$ mixtures. The major conclusions of the study are as follows:

1. Effects of flame stretch on laminar burning velocities could be correlated in terms of the local Karlovitz number to yield $S_{L\infty}/S_L = 1 + \text{MaKa}$, where the Markstein number was a constant for a particular reactant mixture over the available ranges of flame stretch (0–7600 s^{-1} for hydrogen and 0–900 s^{-1} for propane). This yielded either decreasing or increasing laminar burning velocities with increasing Ka at stable or unstable preferential-diffusion conditions.
2. Markstein numbers largely varied with fuel-equivalence ratio for a particular fuel and were in the range -2.7 to 13.3 and -2.2 to 5.5 for freely propagating hydrogen and propane flames, with absolute values progressively increasing as fuel-equivalence ratios move away from the neutral preferential-diffusion condition. The relatively large values of the Markstein numbers imply that laminar burning velocities measured for freely propagating flames in typical laboratory apparatus generally are affected by flame stretch, aside from near-neutral preferential-diffusion conditions, with corresponding significant effects of stretch for turbulent premixed flames.
3. Neutral preferential-diffusion conditions were observed at fuel-equivalence ratios of 1.5–1.6 for both hydrogen and propane flames. This transition condition is shifted toward the unstable side of the maximum laminar burning velocity condition, which the simplest preferential-diffusion theories associate with neutral stability, for both fuels.
4. Transition to cellular flames by hydrodynamic instability was observed for stable preferential-diffusion conditions. Correlation of this transition for $H_2/O_2/N_2$ mixtures was in good agreement with earlier results from Groff [21] for propane–air flames, based on the theoretical ideas of Istratov and Librovich [20]. An effect of Markstein number on this transition could not be resolved over the narrow range of available experimental results (Ma of 2.0–2.7 for $H_2/O_2/N_2$ mixtures and 4.3–5.5 for propane–air mixtures).

5. As expected, transition to irregular flame surfaces for unstable preferential-diffusion conditions occurred at Re_{cr} smaller than those associated with the onset of hydrodynamic instability for stable conditions.
6. Finally, present findings concerning effects of flame stretch on the laminar burning velocities of propane–air flames, based on the measurements of Palm-Leis and Strehlow [5], should be treated as preliminary because it appears likely that fuel-equivalence ratios reported in Ref. 5 are somewhat in error.

This research was supported by the National Science Foundation under Grant No. CTS-9019813. The authors also wish to thank General Motors Research Laboratories, Warren, MI, for donation of the combustion chamber. Finally, the helpful advice of the reviewers is gratefully acknowledged.

REFERENCES

1. Wu, M.-S., Kwon, S., Driscoll, J. F., and Faeth, G. M., *Combust. Sci. Technol.* 73:327–350 (1990).
2. Wu, M.-S., Kwon, S., Driscoll, J. F., and Faeth, G. M., *Combust. Sci. Technol.* 78:69–96 (1991).
3. Kwon, S., Wu, M.-S., Kwon, S., Driscoll, J. F., and Faeth, G. M., *Combust. Flame* 88:221–238 (1992).
4. Wu, M.-S., Kwon, S., Driscoll, J. F., and Faeth, G. M., *Combust. Sci. Technol.* (in press).
5. Palm-Leis, A., and Strehlow, R. A., *Combust. Flame* 13:111–129 (1969).
6. Fristrom, R. M., *Phys. Fluids* 8:273–280 (1965).
7. Deshaies, B., and Cambray, P., *Combust. Flame* 82:361–375 (1990).
8. Law, C. K., Zhu, D. L., and Yu, G., *Twenty-First Symposium (International) on Combustion*, The Combustion Institute, Pittsburgh, 1986, p. 1419.
9. Searby, G., and Quinard, J., *Combust. Flame* 82:298–311 (1990).
10. Markstein, G. H., *Non-Steady Flame Propagation*, Pergamon, New York, 1964, p. 22.
11. Clavin, P., *Prog. Energ. Combust. Sci.* 11:1–59 (1985).
12. Law, C. K., *Twenty-Second Symposium (International) on Combustion*, The Combustion Institute, Pittsburgh, 1988, p. 1381.
13. Peters, N., *Twenty-First Symposium (International) on Combustion*, The Combustion Institute, Pittsburgh, 1986, p. 1231.
14. Strehlow, R. A., and Savage, L. D., *Combust. Flame* 31:209–211 (1978).
15. Clavin, P., and Williams, F. A., *J. Fluid Mech.* 90:589–604 (1979); 116:251–282 (1982).
16. Ronney, P. D., *Combust. Flame* 82:1–14 (1990).
17. Manton, J., von Elbe, G., and Lewis, B., *J. Chem. Phys.* 20:153–157 (1952).
18. Markstein, G. H., *J. Aero. Sci.* 18:199–209 (1951).
19. Markstein, G. H., *J. Chem. Phys.* 20:1051–1052 (1952).
20. Istratov, A. G., and Librovich, V. B., *Astronaut. Acta* 14:453–467 (1969).
21. Groff, E. G., *Combust. Flame* 48:51–62 (1982).
22. Gordon, S., and McBride, B. J., NASA Report SP-273, Washington, 1971.
23. Lewis, B., and von Elbe, G., *Combustion, Flames, and Explosions of Gases*, 2nd ed., Academic, New York, 1961, p. 381.
24. Reid, R. C., Prausnitz, J. M., and Sherwood, T. K., *The Properties of Gases and Liquids*, 3rd ed., McGraw-Hill, New York, 1977, p. 391.
25. Keenan, J. H., Chao, J., and Kaye, J., *Gas Tables*, Wiley, New York, 1980.
26. Harris, M. E., Grumer, J., von Elbe, G., and Lewis, B., *Third Symposium on Combustion, Flame and Explosion Phenomena*, Williams & Wilkins, Baltimore, 1949, p. 80.
27. Yamaoka, I., and Tsuji, H., *Twentieth Symposium (International) on Combustion*, The Combustion Institute, Pittsburgh, 1984, p. 1883.
28. Anderson, J. W., and Fein, R. S., *J. Chem. Phys.* 17:1268–1273 (1949).
29. Scholte, T. G., and Vaags, P. B., *Combust. Flame* 3:495–501 (1959).
30. Gray, K. L., Linnett, J. W., and Mellish, C. E., *Trans. Farad. Soc.* 48:115 (1952).
31. Egerton, A., and Thabet, S. K., *Proc. Soc. Lond. A* 211:445–471 (1952).
32. Badami, G. N., and Egerton, A., *Proc. R. Soc. Lond. A* 228:297–332 (1955).

Received 25 August 1991; revised 13 April 1992